Emergent Fermi-Liquid-Like Phase by Melting a Holon Wigner Crystal in a Doped Mott Insulator on the Kagome Lattice

Xu-Yan Jia(贾旭岩)[1], Wen Huang(黄文)[2,3], D. N. Sheng(盛冬宁)[4*], and Shou-Shu Gong(龚寿书)[2,3*]

[1]*School of Physics, Beihang University, Beijing 100191, China*
[2]*School of Physical Sciences, Great Bay University, Dongguan 523000, China*
[3]*Great Bay Institute for Advanced Study, Dongguan 523000, China*
[4]*Department of Physics and Astronomy, California State University Northridge, Northridge, California 91330, USA*

(Received 28 November 2025; accepted manuscript online 15 January 2026)

The doped quantum spin liquid on the kagome lattice provides a fascinating platform to explore exotic quantum states, such as the reported holon Wigner crystal at low doping. By extending the doping range to $\delta = 0.027$–0.36, we studied the kagome-lattice t-J model using state-of-the-art density matrix renormalization group calculations. On the $L_y = 3$ cylinder (L_y is the number of unit cells along the circumferential direction), we established a quantum phase diagram with an increasing doping level. In addition to the charge density wave states at lower doping levels, we found an emergent Fermi-liquid-like phase by melting the holon Wigner crystal at $\delta \approx 0.15$, which is characterized by the suppression of charge density oscillation and power-law decay of various correlation functions. For a wider $L_y = 4$ cylinder, the bond-dimension extrapolated correlation functions also support such a Fermi-liquid-like state, suggesting its stability with increasing system size. In a narrow doping range near $\delta = 1/3$ for the $L_y = 3$ cylinder, we find a state with an exponential decay of the single-particle correlation, but the other correlation functions preserve the features in the Fermi-liquid-like phase, which may be a precursor of a superconducting state. Nevertheless, this peculiar state near $\delta = 1/3$ disappears for the $L_y = 4$ cylinder, implying a possible lattice-size dependence. Our results reveal quantum melting from a holon Wigner crystal to a Fermi-liquid-like state with increasing hole density and suggest a doping regime to explore superconductivity in future studies.

DOI: 10.1088/0256-307X/43/3/030706 CSTR: 32039.14.0256-307X.43.3.030706

1. Introduction. With the interplay among band topology, geometry frustration, and electronic correlation, kagome-lattice systems realize a fascinating platform to explore exotic quantum states and phenomena.[1–11] Among these, superconductivity (SC) is an important subject. In addition to the intensively studied kagome superconductors AV_3Sb_5(A = K, Rb, Cs),[2–4,8,9] in which the Fermi level lies close to a Van Hove singularity, another route to SC is to dope a quantum spin liquid (QSL) or an antiferromagnetic Mott insulator on the kagome lattice.[12–14] In a study of cuprate superconductors, Anderson proposed that doping a QSL parent state can naturally give rise to an unconventional SC.[15] Furthermore, it has been conjectured that doping a chiral spin liquid may even lead to topological SC through the condensation of paired fractional quasiparticles.[16–18] Recently, there has been unbiased numerical evidence to support superconducting states in doped Mott insulators on the square[19–25] and triangular[26–28] lattices.

For kagome systems, many antiferromagnets have been proposed as candidates for QSL experimentally.[12–14,29] In model studies, the spin-1/2 kagome model with nearest-neighbor (NN) Heisenberg interaction has been identified as hosting a QSL ground state that may be stabilized by geometric frustration and a low coordination number. However, the nature of this state is unclear, and there is a debate between a gapless $U(1)$ QSL and a gapped Z_2 QSL.[30–44] Beyond the NN Heisenberg interaction, remarkably, some additional interactions can drive a Kalmeyer–Laughlin chiral spin liquid with a topological spin Chern number,[45] such as further-neighbor antiferromagnetic interactions[46–48] or three-spin scalar chiral coupling.[49–51]

The discovered QSL states in kagome systems stimulated interest in doping. Early variational Monte Carlo (VMC) studies on the kagome t-J model found that even a small amount of hole doping may drive a zero-flux state with a valence bond crystal (VBC) order, which persists up to a doping level of $\delta \approx 0.18$.[52,53] Later, by considering the $SU(2)$-gauge rotation in the mean-field Hamiltonian, the VMC study obtained a chiral noncentrosymmetric nematic superconducting state at $\delta \lesssim 0.02$, and the VBC state was restored at a higher doping.[54] By contrast, density matrix renormalization group (DMRG) calculations up to $\delta \approx 0.11$ in finite-width cylinder systems yielded an insulating charge density wave (CDW) phase,[55] manifesting itself as a stripe crystal or a Wigner crystal depending on the doping concentration and

*Corresponding authors. Email: shoushu.gong@gbu.edu.cn; donna.sheng1@csun.edu
© 2026 Chinese Physical Society and IOP Publishing Ltd. All rights, including for text and data mining, AI training, and similar technologies, are reserved.

cylinder geometry. Owing to the short-range spin correlation, which is similar to the QSL parent state, this CDW phase is understood to be a crystalline state formed by spinless holons instead of holes.[55–57] With additional chiral coupling, the doped chiral spin liquid also gives rise to CDW states.[56] Interestingly, in the lightly doped extended t-J model, the increase in the next-NN couplings can melt the CDW states and lead to a Fermi-liquid-like phase.[58]

At higher doping levels, many exotic charge uniform states have been theoretically proposed in doped QSLs, such as holon metals, fractionalized Fermi liquids, and SC.[59] Recently, a study employing projected entangled simplex states (PESS) provided new results for the kagome t-J model over a wider doping range.[60] The PESS simulations revealed different types of Wigner crystals depending on the doping level for $\delta \lesssim 0.27$. For a higher doping concentration ($0.27 < \delta < 1/3$), the PESS study obtained uniform states, including a non-Fermi-liquid state characterized by an exponential decay of single-particle and spin correlation functions ($0.27 < \delta < 0.32$) and a pair density wave state ($0.32 < \delta < 1/3$). These novel findings have sparked growing interest in the kagome-lattice t-J model under higher doping.

In this study, we employed DMRG calculations to investigate the kagome-lattice t-J model over a wide doping range of $\delta = 0.027$–0.36. We focused on cylindrical geometry with a circumference of 3 unit cells ($L_y = 3$) and mapped a phase diagram with increasing doping levels, as shown in Fig. 1. At lower doping levels, we confirmed the CDW states reported in previous DMRG calculations.[55,56] At $\delta \approx 0.15$, the CDW order is melted, and the measured correlation functions exhibit substantial enhancement. For $0.15 \lesssim \delta \lesssim 0.36$ (except for a narrow regime near $\delta = 1/3$), we identified a Fermi-liquid-like phase characterized by power-law decay of the measured correlation functions and the absence of hole pairing. In a very narrow doping range near $\delta = 1/3$, the single-particle correlation exhibits exponential decay, but the other correlation functions preserve the features of the Fermi-liquid-like phase. In particular, the SC pairing correlation function is much stronger than the square of the single-particle correlation, which characterizes hole pairing and thus suggests that this state is a possible precursor of a superconducting state, such as the pseudogap state. In the wider $L_y = 4$ system, the Fermi-liquid-like state is supported by the correlation functions, but the emergent state near 1/3 doping disappears, suggesting that this phase may have a lattice size dependence. In the summary section, we discuss future studies on the phase transition of melting the holon Wigner crystal and potential routes to search for the SC near $\delta = 1/3$ by considering other interactions.

2. Model and Method. The Hamiltonian of the kagome-lattice t-J model is given as

$$H = -t \sum_{\langle ij \rangle, \sigma} (\hat{c}^{\dagger}_{i,\sigma} \hat{c}_{j,\sigma} + \text{H.c.}) + J \sum_{\langle ij \rangle} \left(\hat{\boldsymbol{S}}_i \cdot \hat{\boldsymbol{S}}_j - \frac{1}{4} \hat{n}_i \hat{n}_j \right),$$

where $\hat{c}^{\dagger}_{i,\sigma}$ and $\hat{c}_{i,\sigma}$ are the creation and annihilation operators, respectively for an electron with spin σ ($\sigma = \pm 1/2$) at the site i, $\hat{\boldsymbol{S}}_i$ is the spin-1/2 operator, and $\hat{n}_i \equiv \sum_{\sigma} \hat{c}^{\dagger}_{i,\sigma} \hat{c}_{i,\sigma}$ is the electron number operator. The t-J model enforces the no-double-occupancy constraint at each site. In this study, we consider a system with NN couplings t and J in the doping range $\delta = 0.027$–0.36, and we set $t/J = 3$ to mimic the large Hubbard-U case.

To determine the ground state of this model, we performed DMRG[61] calculations on the cylindrical lattice, as illustrated in Fig. 1(a), where $\boldsymbol{e}_1$ and $\boldsymbol{e}_2$ denote the two unit vectors. We employed a kagome Y-cylinder (YC) with periodic (open) boundary conditions along the $\boldsymbol{e}_2$ ($\boldsymbol{e}_1$) direction. We denote the number of unit cells along the $\boldsymbol{e}_2$ and $\boldsymbol{e}_1$ directions as L_y and L_x, respectively. Note that we added an extra column of lattice sites to the right boundary, where each unit cell contained only A and C sites, as shown in Fig. 1(a). This YC cylinder with modified boundary conditions can reduce the open boundary effects. Therefore, the lattice has $2L_x + 1$ columns and $2L_y$ rows, with the column indices ranging as $x \in [1, 2L_x + 1]$ and the row indices ranging as $y \in [1, 2L_y]$. We denote the cylinders as YC$2L_y$, with a total site number $N = 3L_yL_x + 2L_y$. The doping ratio δ is defined as $\delta = N_{\text{h}}/N$, where N_{h} is the number of doped holes. We mainly studied the YC6 cylinder ($L_y = 3$) with $L_x = 32$, and examined the YC8 cylinder for some typical parameter points. By combining the charge $U(1)$ and spin $SU(2)$ symmetries,[62]

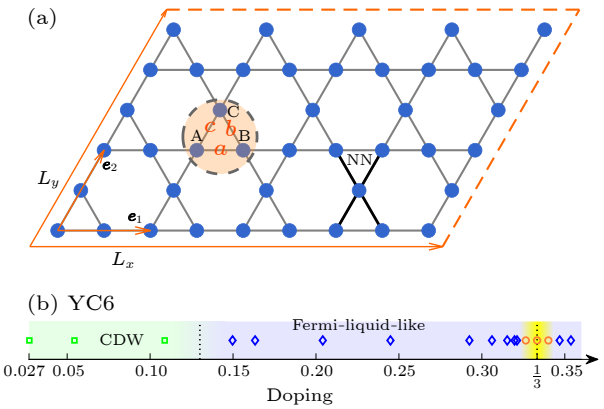

Fig. 1. Schematic of the kagome-lattice t-J model and quantum phase diagram of the YC6 system with increasing doping ratio $\delta = 0.027$–0.36. (a) t-J model on the kagome Y-cylinder (YC), where periodic and open boundary conditions are imposed along the directions specified by the lattice vectors $\boldsymbol{e}_2$ and $\boldsymbol{e}_1$. Electrons and doped holes reside at the lattice vertices (solid circles). Each unit cell (denoted by a small triangle in the shaded region) contains three sites (A, B, and C) and three bonds (a, b, and c). L_x and L_y are the numbers of unit cells along the $\boldsymbol{e}_1$ and $\boldsymbol{e}_2$ directions, respectively. The column and row indices (x, y) were used later to specify the coordinates of the individual lattice sites. In the example illustrated in the figure, sites A and B correspond to the coordinates $(3, 3)$ and $(4, 3)$, respectively. (b) Quantum phase diagram of the kagome-lattice t-J model ($t/J = 3$) in the YC6 ($L_y = 3$) system. In addition to the charge density wave (CDW) states observed previously,[55,56] we identified a new Fermi-liquid-like phase. In the narrow regime near 1/3 doping, the state shows an exponential decay of the single-particle correlation, but the other correlation functions retain the features of the Fermi-liquid-like phase.

we maintained bond dimensions up to $D = 28000$ $SU(2)$ multiplets, which are equivalent to approximately 84000 $U(1)$ states. For all the parameter points in this study, the DMRG truncation error of the largest bond dimension was controlled below 2×10^{-7}, yielding accurate results.

3. Charge Density Wave and Fermi-Liquid-Like Phase. Figure 1(b) shows the phase diagram of the YC6 system. In the doping range $\delta = 0.027$–0.11, previous DMRG studies found insulating CDW states.[55,56] In this study, we further investigate higher doping levels and identify a Fermi-liquid-like phase in the doping range $\delta \approx 0.15$–0.36, with the exception of $\delta \approx 1/3$.

The CDW and Fermi-liquid-like phases can be distinguished by their charge density distributions and correlation functions. In the CDW phase, the charge density distribution shows a striped crystal or Wigner crystal, depending on the lattice geometry and doping ratio.[55,56] The CDW states exhibit a stable charge density oscillation with a relatively large amplitude. The superconducting, single-particle, and spin-spin correlation functions demonstrate exponential decay in this phase with very small correlation lengths.[55,56] Upon increasing the doping level, the emergent Fermi-liquid-like phase displayed strikingly different characteristics. The charge density distribution becomes uniform along the $\boldsymbol{e}_2$ direction, and along the $\boldsymbol{e}_1$ direction, it exhibits an extremely small oscillation amplitude, characterizing the melted static CDW order. Moreover, the correlation functions display a power-law decay rather than an exponential decay. In particular, the magnitude of the SC pairing correlation was comparable to the square of the single-particle correlation, indicating the absence of hole pairing. The finite central charge obtained by fitting the entanglement entropy also supported its gapless nature. These features consistently characterize this new phase as a Fermi-liquid-like state.

3.1. Charge Density Profiles on YC6. First, we present the charge density distributions of YC6 in Fig. 2. The electron density at each lattice site (x, y) is denoted by $n(x, y)$, where x (y) is the lattice index along the direction $\boldsymbol{e}_1$ ($\boldsymbol{e}_2$), with the NN distance as the unit of length. When the electron density was uniform along the $\boldsymbol{e}_2$-direction, we employed the column-averaged electron density, defined as $n_x \equiv \frac{1}{N_y}\sum_{y=1}^{N_y} n(x, y)$, where $N_y = 2L_y$ ($N_y = L_y$) for odd (even) x.

At $\delta \approx 0.11$, the CDW manifests as a Wigner crystal,[55,56] as shown in Fig. 2(a). Here, we employed the hole distribution $n_{\rm h}(x, y) = 1 - n(x, y)$ to highlight the visual effects. The holes formed a spot-like pattern with a density modulation amplitude ≈0.07, indicating the formation of a larger unit cell. The number of doped holes exactly matched the number of yellow spots in Fig. 2(a), demonstrating that, on average, each emergent unit cell contains one hole. In the CDW phase, the emergent unit cells do not exhibit a fixed pattern but depend on the lattice geometry and doping ratio. For example, in the YC6 cylinder, in addition to the spot-like pattern shown in Fig. 2(a), the hole density distributions form stripe-like patterns at $\delta = 1/36$–$1/18$,[55] with the number of emergent unit cells remaining equal to the number of doped holes.

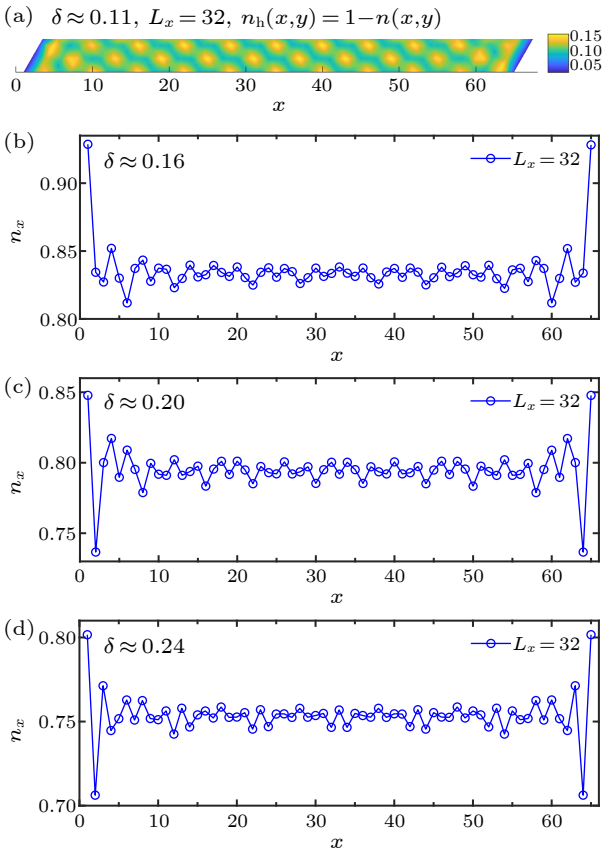

Fig. 2. Charge density profiles of YC6 systems with $L_x = 32$. $n(x, y)$ denotes the electron density at each lattice site, where x (y) is the lattice index along the $\boldsymbol{e}_1$ ($\boldsymbol{e}_2$) direction, with the NN distance as the unit of length. The column-averaged electron density is denoted as n_x. (a) Hole density distribution $n_{\rm h}(x, y) = 1 - n(x, y)$ for $\delta \approx 0.11$ in the CDW phase. (b)–(d) n_x in Fermi-liquid-like phase at $\delta \approx 0.16$, 0.20, and 0.24.

In the doping range $\delta \gtrsim 0.15$, the charge density distribution becomes uniform along the $\boldsymbol{e}_2$ direction; therefore, we analyze the column-averaged density $n(x)$ as shown in Figs. 2(b)–2(d). Along the $\boldsymbol{e}_1$ direction, the charge density oscillation was significantly suppressed, which, in the open boundary conditions, strongly suggests the absence of a static CDW order. In the Supplementary Material (SM), we show the distribution of the average charge density per unit cell.

3.2. Correlation Functions on YC6. In this subsection, we present the DMRG results for the correlation functions. First, we begin by analyzing the spin-singlet pairing correlation function $P_{\alpha\beta}(r) = \langle \hat{\Delta}^\dagger_\alpha(i_0)\hat{\Delta}_\beta(i_0 + r)\rangle$, where i_0 denotes the reference site at 1/4 length of the cylinder and r denotes the number of sites away from i_0 along the $\boldsymbol{e}_1$ direction. The spin-singlet pair-field creation operator $\hat{\Delta}^\dagger_\alpha(i)$ is defined as $\hat{\Delta}^\dagger_\alpha(i) = 1/\sqrt{2}(\hat{c}^\dagger_{i\uparrow}\hat{c}^\dagger_{i+\alpha\downarrow} - \hat{c}^\dagger_{i\downarrow}\hat{c}^\dagger_{i+\alpha\uparrow})$, where α denotes the three bond directions: $\boldsymbol{a}$, $\boldsymbol{c}$, and $\boldsymbol{b}$, which correspond to $\boldsymbol{e}_1/2$, $\boldsymbol{e}_2/2$, and $(\boldsymbol{e}_2 - \boldsymbol{e}_1)/2$, respectively [see Fig. 1(a)]. Figure 3(a) shows P_{aa} for $\delta \approx 0.11$–0.32, where $\xi_{\rm sc}$ and $K_{\rm sc}$ are the fitting exponents obtained in the exponential decay function and power-law decay function, respectively. The pairing correlation exhibited a substantial enhancement from the CDW phase to the Fermi-liquid-like

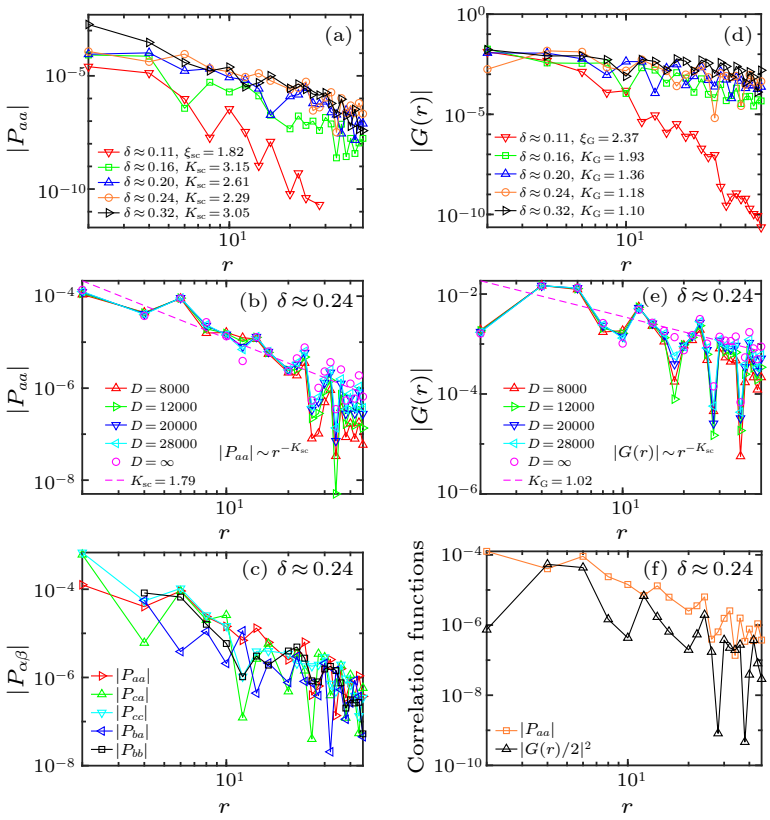

Fig. 3. The SC pairing correlations and single-particle correlations $G(r)$ in the YC6 system. (a) $|P_{aa}|$ at various doping levels. $\xi_{\rm sc}$ and $K_{\rm sc}$ are the fitted exponential and power-law decay exponents, respectively. (b) $|P_{aa}|$ for $\delta \approx 0.24$ with different bond dimensions ranging from $D = 8000$–28000. The dashed line denotes the power-law fit of the extrapolated $D \to \infty$ results. (c) Pairing correlation functions of different bonds $|P_{\alpha\beta}(r)|$ at $\delta \approx 0.24$. (d) and (e) are the similar plots for the single-particle Green's function $G(r)$. (f) Comparison of pairing correlation $|P_{aa}|$ with the square of single-particle correlation $|G(r)/2|^2$ at $\delta \approx 0.24$.

phase. For $\delta \approx 0.24$, we analyzed the results obtained for different bond dimensions (up to $D = 28000$) and extrapolated the results to the $D \to \infty$ limit using a polynomial function of the bond dimension. The extrapolated pairing correlation can be fitted well by a power-law decay with the power exponent $K_{\rm sc} \approx 1.79$ [Fig. 3(b)]. We also examined other pairing correlation functions including P_{bb}, P_{cc}, P_{ca}, and P_{ba} [Fig. 3(c)] that have similar magnitudes and power exponents. For simplicity, we demonstrate the results for P_{aa} as representative.

Next, we examined the single-particle Green's function $G(r) = \sum_\sigma \langle \hat{c}^\dagger_{i_0,\sigma} \hat{c}_{i_0+r,\sigma} \rangle$. In the CDW phase, $G(r)$ decays exponentially [Fig. 3(d)], which characterizes the charge insulating phase. In the Fermi-liquid-like phase, $G(r)$ increases significantly and decays algebraically. Similarly, we extracted the $D \to \infty$ results. For $\delta \approx 0.24$, the extrapolated $G(r)$ fits the power-law decay well with the power exponent $K_{\rm G} \gtrsim 1$ [see Fig. 3(e)], indicating a gapless single-particle excitation. To further clarify the nature of the pairing, we compare P_{aa} with the square of the single-particle correlation $(G(r)/2)^2$ and find that the two quantities are very close [Fig. 3(f)], indicating the absence of hole pairing.

Next, we present the results of the density correlation function $D(r) = \langle \hat{n}_{i_0} \hat{n}_{i_0+r} \rangle - \langle \hat{n}_{i_0} \rangle \langle \hat{n}_{i_0+r} \rangle$. At $\delta \approx 0.11$, the charge density profile exhibits a Wigner crystal feature with spontaneous translational symmetry breaking in both $\boldsymbol{e}_1$ and $\boldsymbol{e}_2$ directions [Fig. 2(a)]. In this state, our defined density correlation function can describe the charge density fluctuations. In the Fermi-liquid-like phase, the static CDW order disappears [Figs. 2(b)–2(d)], and the density correlation function describes the charge order. As shown in Fig. 4(a), the decay of $D(r)$ can be fitted algebraically with the power exponent $K_{\rm cdw} \approx 2$, which is consistent with the Fermi-liquid-like state. Analysis of the bond dimension dependence shows a very good convergence of the density correlation function [Fig. 4(b)].

The spin-correlation function $S(r) = \langle \boldsymbol{S}_{i_0} \cdot \boldsymbol{S}_{i_0+r} \rangle$ exhibits exponential decay with a short correlation length in the CDW phase [Fig. 4(c) and Ref. [55]]. In the Fermi-liquid-like phase, the spin correlation was significantly enhanced and appeared to decay algebraically. Through bond dimension extrapolation, the well-converged spin-correlation function can fit a power-law decay with the exponent $K_{\rm s} \approx 2.4$ for $\delta \approx 0.24$ [Fig. 4(d)]. These correlation function results agree with a Fermi-liquid-like state.

3.3. Entanglement Entropy on YC6. In this subsection, we calculate the entanglement entropy and fit the central charge to characterize the gapless nature of the Fermi-liquid-like phase. The entanglement entropy between two subsystems is defined as $S_{\rm E}(l) = -{\rm Tr}[\rho(l) \ln \rho(l)]$ $(1 \le l \le L_x - 1)$, where l and $L_x - l$ are the lengths of the two subsystems and $\rho(l)$ is the reduced density matrix of subsystem l obtained from the

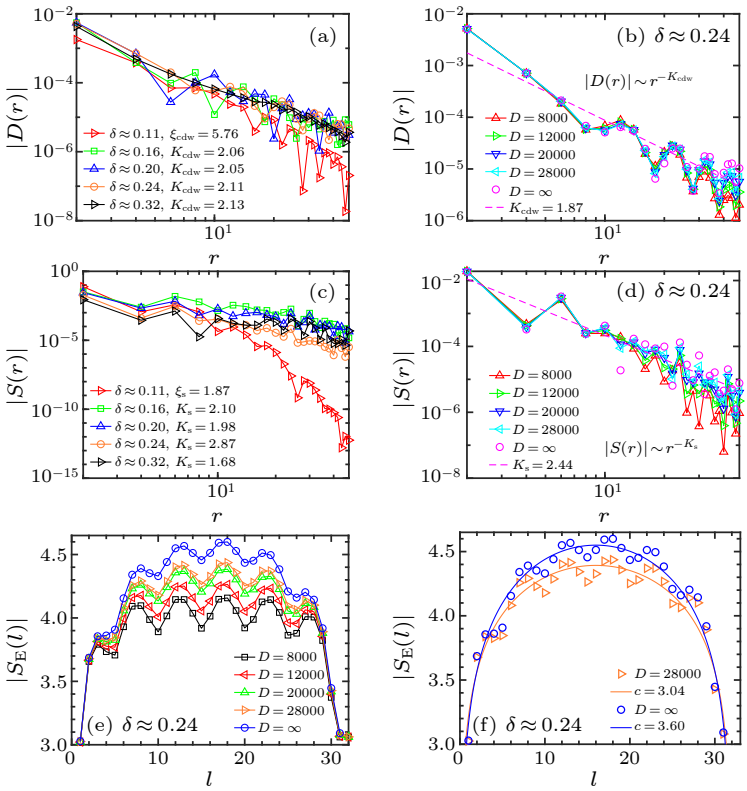

Fig. 4. Density correlation $D(r)$, spin correlation $S(r)$, and entanglement entropy S_E in YC6 systems with $L_x = 32$. (a) $|D(r)|$ for different doping levels. (b) $|D(r)|$ for $\delta \approx 0.24$ for different bond dimensions $D = 8000$–28000. (c) and (d) show similar plots for spin correlation $S(r)$. (e) Entanglement entropy for $\delta \approx 0.24$ for different bond dimensions. The $D = \infty$ results are extrapolated from the finite bond-dimension data. Label l denotes the unit cell index along the $\boldsymbol{e}_1$ direction. (f) Fitting of the central charge c from the formula $S_E(l) = (c/6)\ln[(L_x/\pi)\sin(l\pi/L_x)] + g$ for $D = 28000$ and $D = \infty$ data, yielding a finite central charge.

ground state of the entire system. According to conformal field theory, for one-dimensional critical systems with open boundary conditions, the bipartite entanglement entropy S_E follows the formula $S_E(l) = (c/6)\ln[(L_x/\pi)\sin(l\pi/L_x)] + g$, where c is the central charge, L_x is the length of the entire system, and g is a nonuniversal constant.[63] In Fig. 4(e), we show the entanglement entropy S_E for $\delta \approx 0.24$ on a $L_x = 32$ cylinder. With increasing bond dimensions, S_E continues to grow. For the entropy at each given l, we extrapolated the $D \to \infty$ result from the DMRG data obtained using different bond dimensions (see SM). In Fig. 4(f), we fit the entropy data to extract the central charge. For $D = 28000$, we find $c \approx 3$, and for $D \to \infty$ we obtain $c \approx 3.6$. Note that to determine the central charge, the system length must be enlarged, and the central charge in the $L_x \to \infty$ limit must be extracted. Limited by computational costs, the value of the central charge determined may not be accurate, but its finite value clearly characterizes the gapless nature of this state. In the conformal field theory, the value of the central charge c corresponds to the number of gapless modes in the system. Our fitting results suggest that there may be three gapless modes in the Fermi-liquid-like state of the YC6 cylinder.

3.4. DMRG Results on YC8. We further studied a wider YC8 system to examine the finite-size effects and gain insight into the ground state within the two-dimensional limit. In Figs. 5(a)–5(d), we present the single-particle Green's function $G(r)$ and the spin correlation $S(r)$ of the YC8 system at $\delta \approx 0.24$, which were obtained with bond dimensions $D = 12000$–20000. Here, the bond dimensions are smaller than $D = 28000$ on YC6 owing to computational cost. We extrapolated the data with respect to the bond dimensions to estimate the results within the $D \to \infty$ limit. In this extrapolation, we discarded the data points that oscillated with the bond dimensions. To analyze the decay behavior of the correlation functions, we considered both double–logarithmic and semi–logarithmic fitting. For $G(r)$, power-law fitting up to a distance $r \sim 30$ yielded an exponent $K_G \approx 1.03$ [Fig. 5(a)], and exponential fitting yielded a correlation length $\xi_G \approx 12.6$ [Fig. 5(b)], indicating a slow decay of $G(r)$. For $S(r)$, the power-law fitting yielded $K_s \approx 2.95$ [Fig. 5(c)], and the exponential fitting obtained was $\xi_s \approx 4.1$ [Fig. 5(d)].

To analyze the size dependence, we compared the results of the YC6 and YC8 systems at $\delta \approx 0.24$ for both $G(r)$ [Fig. 5(e)] and $S(r)$ [Fig. 5(f)]. Overall, the results of the two systems are consistent, and only the longer-distance correlations ($r \gtrsim 25$) of the YC8 system show a more pronounced decreasing trend, which may be due to lower convergence. By maintaining larger bond dimensions, one can expect an enhancement in long-distance data. As an estimate, we also show the extrapolated $D \to \infty$ results for YC8, which are consistent with the YC6 results.

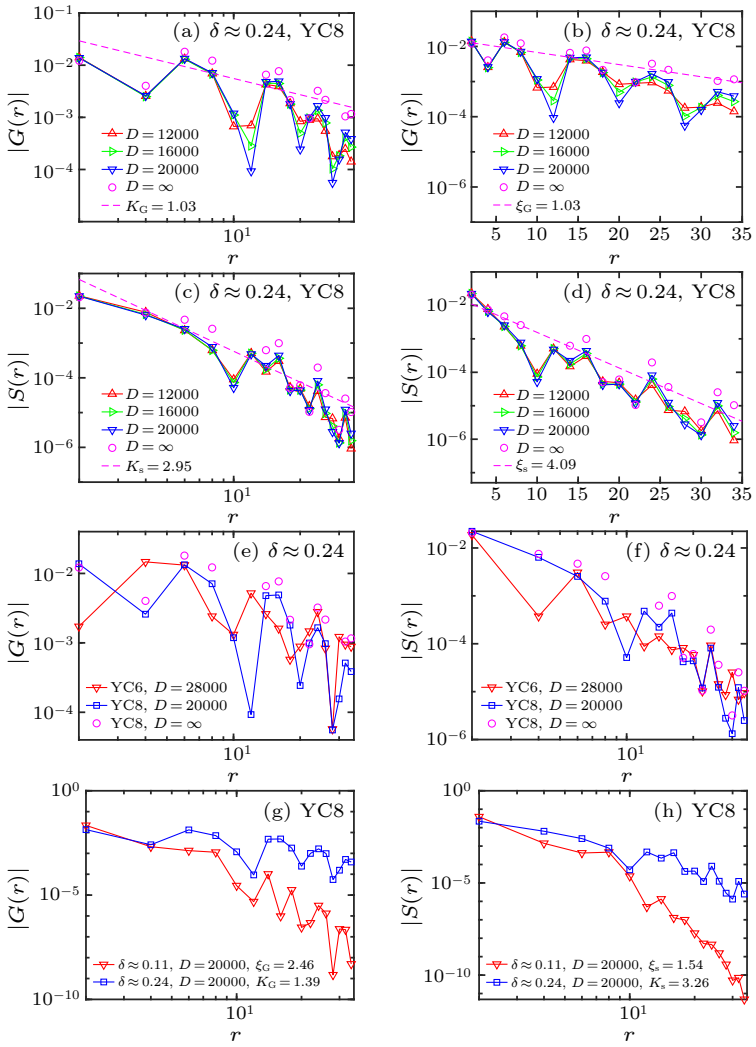

Fig. 5. Single-particle Green's function $G(r)$ and spin correlation $S(r)$ in the YC8 system. (a) Double-logarithmic plot and (b) semi-logarithmic plot of $G(r)$ for $\delta \approx 0.24$ on the YC8 cylinder with bond dimensions $D = 12000$–20000. (c) and (d) are similar plots of spin correlation $S(r)$. (e) and (f) are comparison of $G(r)$ and $S(r)$ between the YC6 and YC8 cylinders at $\delta \approx 0.24$. (g) and (h) are comparison of $G(r)$ and $S(r)$ at $\delta \approx 0.11$ and $\delta \approx 0.24$ for the YC8 cylinder.

To distinguish between the CDW and Fermi-liquid-like states on YC8, we compared the correlation functions at $\delta \approx 0.11$ and $\delta \approx 0.24$, as shown in Figs. 5(g) and 5(h). Both $G(r)$ and $S(r)$ decay exponentially with short correlation lengths at $\delta \approx 0.11$ but are enhanced by several orders of magnitude at $\delta \approx 0.24$. These features are consistent with our observations of the YC6 cylinder. Although the YC8 results may be less convergent, the systematic comparisons in Fig. 5 suggests a stable Fermi-liquid-like state with a larger system size.

4. The Quantum States near 1/3 *Doping.* In this section, we focus on the DMRG results near 1/3 doping. Because our DMRG simulations study the ground state in a sector with a total spin quantum number $S = 0$, the number of holes can only be changed by even numbers. Here, we investigated the doping ratio $\delta = 1/3$ (33.33%) and nearby doping levels that differ by two holes (32.65% and 34.01%) and four holes (31.97% and 34.69%). The results are presented in Fig. 6.

For YC6, the charge density profile is nearly uniform at $\delta = 1/3$ [Fig. 6(a)], indicating the absence of a static CDW order. The doping dependence of single-particle correlation [Fig. 6(b)] shows that $|G(r)|$ are suppressed at $\delta = 32.65\%$, 33.33%, and 34.01%. In particular, $|G(r)|$ exhibits a pronounced drop at $\delta = 1/3$, which behaves as an exponential decay. At a higher $\delta = 34.69\%$, $|G(r)|$ quickly recovers its magnitude in the Fermi-liquid-like phase. This observation suggests a new state in the narrow doping range near $\delta = 1/3$ that appears to open a single-particle gap.

To clarify the nature of this state further, we compared the square of the single-particle correlation to that of the pairing correlation. As shown in Fig. 6(c), the pairing correlation is much stronger than $|G(r)/2|^2$ at $\delta = 1/3$, suggesting hole pairing. At $\delta = 31.97\%$ and 34.69%, the two quantities exhibit comparable magnitudes, as illustrated in Figs. 6(d) and 6(e), which agrees with the expected features of the Fermi-liquid-like phase. In addition, we compared the spin correlation function at $\delta = 1/3$ with that in the Fermi-liquid-like phase, which shows no qualitative

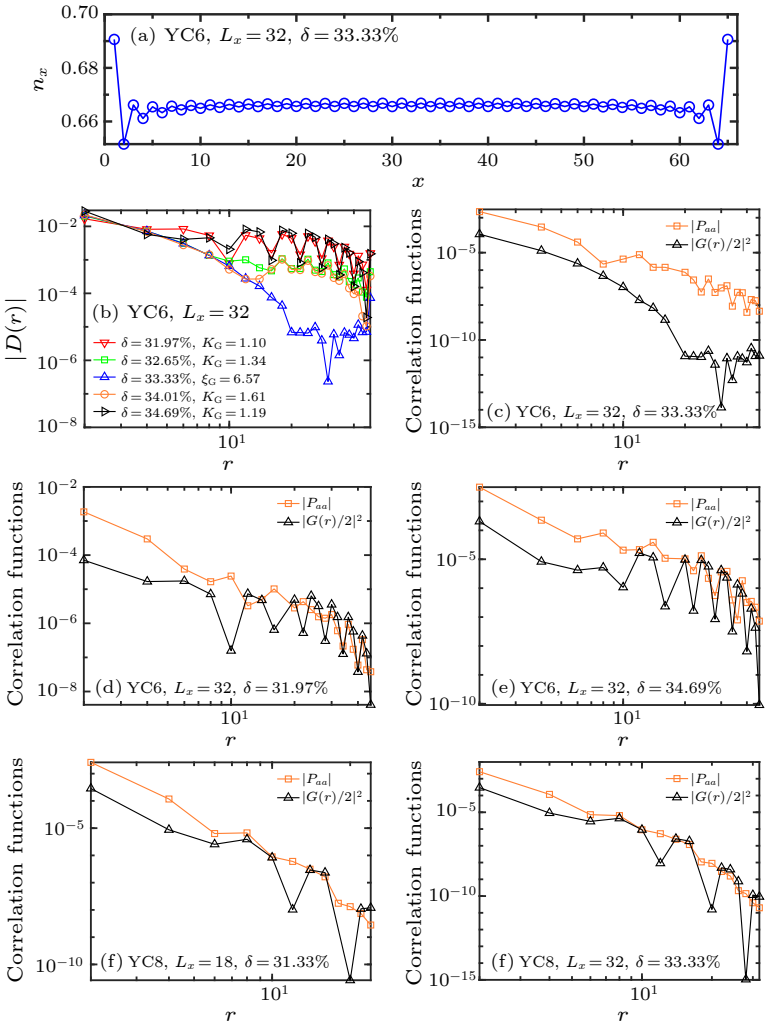

Fig. 6. Charge density profiles and correlation functions around 1/3-doping. (a) Charge density profiles at $\delta = 1/3$. (b) Single-particle Green's function $G(r)$ for several doping levels around $\delta = 1/3$. (c)–(e) Comparison between the pairing correlation $|P_{aa}|$ and square of the single-particle Green's function $|G(r)/2|^2$ at $\delta = 1/3$, 31.97%, and 34.69%. The quantities in (a)–(e) were measured on a YC6 cylinder with bond dimensions $D = 16000$. (f) and (g) are comparison between the pairing correlation $|P_{aa}|$ and the square of the single-particle Green's function $|G(r)/2|^2$ at $\delta = 1/3$ on the YC8 cylinder with $L_x = 18$ ($D = 24000$) and $L_x = 32$ ($D = 16000$), respectively. Notably, in the calculations of (f) and (g), we used a regular cylindrical geometry without the additional right boundary, which allows precise 1/3 doping on the YC8 cylinder.

difference and indicates that the spin modes remain gapless at $\delta = 1/3$ [see SM]. The correlation function results describe this state as a possible precursor of a superconducting state, such as a pseudogap state.

We further examined 1/3 doping on the YC8 cylinder but found that the character of the hole pairing disappears. The magnitudes of the squared single-particle and pairing correlations are comparable [Figs. 6(f) and 6(g)] for the YC8 cylinder. This indicates that the state near 1/3 doping in the YC6 system may have a system-size dependence, which requires further study.

5. Summary and Discussion. Using DMRG calculations, we investigated the kagome-lattice t-J model at $\delta = 0.027$–0.36, which extends the doping range considered in previous DMRG studies.[55,56] On the YC6 cylinder, the system showed a transition from CDW states to a Fermi-liquid-like phase at $\delta \approx 0.15$. In this metallic phase, the charge density oscillation is suppressed, and the measured correlation functions, including single-particle, spin-spin, density-density, and pairing correlations, decay algebraically. Furthermore, this state is characterized by the existence of gapless modes and the absence of hole pairing. On a wider YC8 cylinder, the bond-dimension extrapolated ($D \to \infty$) correlation functions also support such a Fermi-liquid-like state, suggesting its stability with increasing system size. Nonetheless, because of the three-sublattice structure of the kagome lattice, we may not obtain the Fermi surface properties, such as quasi-particle residue, based on the current results.

Remarkably, this state, with an algebraic single-particle correlation, is distinct from the non-Fermi liquid state found in the PESS simulation,[60] which shows an exponential decay of the single-particle and spin correlations.[59] While the phase transition from a Wigner crystal to a Fermi liquid with increasing electron density is conventional in an electron gas,[64–66] the transition from a

holon Wigner crystal with fractionalization to a Fermi liquid may be highly nontrivial and has been intensively studied in related models of bilayer transition metal dichalcogenide materials.[67,68] It would be very interesting to clarify the nature of this Fermi-liquid-like phase, for example, a conventional Fermi liquid or a fractionalized Fermi liquid, and the transition properties during the melting of the holon Wigner crystal. We leave these open questions to future studies, including the mapping of the Fermi surface topology and probing the topological order of the fractionalized Fermi liquid.

Near 1/3-doping on the YC6 cylinder, the state with an exponential decay of the single-particle correlation may be considered a precursor of a superconducting state, similar to the pseudogap state. This state may be connected to the pair-density wave state found in the PESS simulation at $\delta \in [0.32, 1/3]$.[60] Nevertheless, owing to the size dependence observed in the YC6 and YC8 systems, this doping range requires further study with larger system sizes. In addition, considering additional interactions, such as spin-chiral interactions, flux, or density-density attraction, may be helpful for stabilizing a superconducting phase near 1/3 doping.

Acknowledgements. X. Y. J. and S. S. G. were supported by the National Natural Science Foundation of China (Grant Nos. 12274014 and 12534009), the Guangdong Provincial Quantum Science Strategic Initiative (Grant No. GDZX2501006), the Special Project in Key Areas for Universities in Guangdong Province (Grant No. 2023ZDZX3054), and the Dongguan Key Laboratory of Artificial Intelligence Design for Advanced Materials. D. N. S. was supported by the U.S. Department of Energy, Office of Basic Energy Sciences (Grant No. DE-FG02-06ER46305) for DMRG studies on unconventional superconductivity. Computational resources were supported by the SongShan Lake HPC Center (SSL-HPC) at Great Bay University (X. Y. J. and S. S. G.). The numerical simulation was supported in part by the US National Science Foundation (Grant No. DMR-2406524) (D. N. S.).

References

[1] Wang Y, Wu H, McCandless G T, Chan J Y, and Ali M N 2023 *Nat. Rev. Phys.* **5** 635
[2] Yin J X, Lian B, and Hasan M Z 2022 *Nature* **612** 647
[3] Wilson S D and Ortiz B R 2024 *Nat. Rev. Mater.* **9** 420
[4] Jiang K, Wu T, Yin J X, Wang Z, Hasan M Z, Wilson S D, Chen X, and Hu J 2022 *Natl. Sci. Rev.* **10** nwac199
[5] Kanagaraj M, Ning J, and He L 2022 *Rev. Phys.* **8** 100072
[6] Morali N, Batabyal R, Nag P K, Liu E, Xu Q, Sun Y, Yan B, Felser C, Avraham N, and Beidenkopf H 2019 *Science* **365** 1286
[7] Liu D F, Liang A J, Liu E K, Xu Q N, Li Y W, Chen C, Pei D, Shi W J, Mo S K, Dudin P, Kim T, Cacho C, Li G, Sun Y, Yang L X, Liu Z K, Parkin S S P, Felser C, and Chen Y L 2019 *Science* **365** 1282
[8] Zhao H, Li H, Ortiz B R, Teicher S M L, Park T, Ye M, Wang Z, Balents L, Wilson S D, and Zeljkovic I 2021 *Nature* **599** 216
[9] Chen H, Yang H, Hu B, Zhao Z, Yuan J, Xing Y, Qian G, Huang Z, Li G, Ye Y, Ma S, Ni S, Zhang H, Yin Q, Gong C, Tu Z, Lei H, Tan H, Zhou S, Shen C, Dong X, Yan B, Wang Z, and Gao H J 2021 *Nature* **599** 222
[10] Yin J X, Ma W, Cochran T A, Xu X, Zhang S S, Tien H J, Shumiya N, Cheng G, Jiang K, Lian B, Song Z, Chang G, Belopolski I, Multer D, Litskevich M, Cheng Z J, Yang X P, Swidler B, Zhou H, Lin H, Neupert T, Wang Z, Yao N, Chang T R, Jia S, and Hasan M Z 2020 *Nature* **583** 533
[11] Nakatsuji S, Kiyohara N, and Higo T 2015 *Nature* **527** 212
[12] Savary L and Balents L 2016 *Rep. Prog. Phys.* **80** 016502
[13] Zhou Y, Kanoda K, and Ng T K 2017 *Rev. Mod. Phys.* **89** 025003
[14] Broholm C, Cava R J, Kivelson S A, Nocera D G, Norman M R, and Senthil T 2020 *Science* **367** eaay0668
[15] Anderson P W 1987 *Science* **235** 1196
[16] Laughlin R B 1988 *Phys. Rev. Lett.* **60** 2677
[17] Wen X G, Wilczek F, and Zee A 1989 *Phys. Rev. B* **39** 11413
[18] Lee D H and Fisher M P A 1989 *Phys. Rev. Lett.* **63** 903
[19] Jiang H C and Kivelson S A 2021 *Phys. Rev. Lett.* **127** 097002
[20] Gong S S, Zhu W, and Sheng D N 2021 *Phys. Rev. Lett.* **127** 097003
[21] Jiang S T, Scalapino D J, and White S R 2021 *Proc. Natl. Acad. Sci. U.S.A.* **118** e2109978118
[22] Lu X, Chen F, Zhu W, Sheng D N, and Gong S S 2024 *Phys. Rev. Lett.* **132** 066002
[23] Chen F, Haldane F D M, and Sheng D N 2025 *Proc. Natl. Acad. Sci. U.S.A.* **122** e2420963122
[24] Jiang H C, Kivelson S A, and Lee D H 2023 *Phys. Rev. B* **108** 054505
[25] Jiang Y F, Devereaux T P, and Jiang H C 2024 *Phys. Rev. B* **109** 085121
[26] Jiang Y F and Jiang H C 2020 *Phys. Rev. Lett.* **125** 157002
[27] Huang Y X and Sheng D N 2022 *Phys. Rev. X* **12** 031009
[28] Huang Y X, Gong S S, and Sheng D N 2023 *Phys. Rev. Lett.* **130** 136003
[29] Norman M R 2016 *Rev. Mod. Phys.* **88** 041002
[30] Ran Y, Hermele M, Lee P A, and Wen X G 2007 *Phys. Rev. Lett.* **98** 117205
[31] Zhu W, Gong S S, and Sheng D N 2025 *Quantum Frontiers* **4** 11
[32] Iqbal Y, Becca F, and Poilblanc D 2011 *Phys. Rev. B* **84** 020407
[33] Iqbal Y, Becca F, Sorella S, and Poilblanc D 2013 *Phys. Rev. B* **87** 060405
[34] Iqbal Y, Poilblanc D, and Becca F 2014 *Phys. Rev. B* **89** 020407
[35] Yan S, Huse D A, and White S R 2011 *Science* **332** 1173
[36] Jiang H C, Weng Z Y, and Sheng D N 2008 *Phys. Rev. Lett.* **101** 117203
[37] Liao H J, Xie Z Y, Chen J, Liu Z Y, Xie H D, Huang R Z, Normand B, and Xiang T 2017 *Phys. Rev. Lett.* **118** 137202
[38] Läuchli A M, Sudan J, and Moessner R 2019 *Phys. Rev. B* **100** 155142
[39] Sun R Y, Jin H K, Tu H H, and Zhou Y 2024 *npj Quantum Mater.* **9** 16
[40] Zhu W, Chen X, He Y C, and Witczak-Krempa W 2018 *Sci. Adv.* **4** eaat5535
[41] Đurić T, Chung J H, Yang B, and Sengupta P 2025 *Phys. Rev. X* **15** 011047
[42] Depenbrock S, McCulloch I P, and Schollwöck U 2012 *Phys. Rev. Lett.* **109** 067201
[43] He Y C, Zaletel M P, Oshikawa M, and Pollmann F 2017 *Phys. Rev. X* **7** 031020
[44] Messio L, Bernu B, and Lhuillier C 2012 *Phys. Rev. Lett.* **108** 207204
[45] Kalmeyer V and Laughlin R B 1987 *Phys. Rev. Lett.* **59** 2095
[46] Gong S S, Zhu W, and Sheng D N 2014 *Sci. Rep.* **4** 6317

[47] Gong S S, Zhu W, Balents L, and Sheng D N 2015 *Phys. Rev. B* **91** 075112
[48] He Y C, Sheng D N, and Chen Y 2014 *Phys. Rev. Lett.* **112** 137202
[49] Bauer B, Cincio L, Keller B P, Dolfi M, Vidal G, Trebst S, and Ludwig A W W 2014 *Nat. Commun.* **5** 5137
[50] Hu W J, Zhu W, Zhang Y, Gong S, Becca F, and Sheng D N 2015 *Phys. Rev. B* **91** 041124
[51] Haghshenas R, Gong S S, and Sheng D N 2019 *Phys. Rev. B* **99** 174423
[52] Guertler S and Monien H 2011 *Phys. Rev. B* **84** 174409
[53] Guertler S and Monien H 2013 *Phys. Rev. Lett.* **111** 097204
[54] Jiang Y F, Yao H, and Yang F 2021 *Phys. Rev. Lett.* **127** 187003
[55] Jiang H C, Devereaux T, and Kivelson S A 2017 *Phys. Rev. Lett.* **119** 067002
[56] Peng C, Jiang Y F, Sheng D N, and Jiang H C 2021 *Adv. Quantum Technol.* **4** 2000126
[57] Kivelson S A, Rokhsar D S, and Sethna J P 1987 *Phys. Rev. B* **35** 8865
[58] Jia X Y, Yang F, Sheng D N, and Gong S S 2025 *Phys. Rev. B* **112** 245145
[59] Law K T and Lee P A 2017 *Proc. Natl. Acad. Sci. U.S.A.* **114** 6996
[60] Xu Z T, Gu Z C, and Yang S 2024 arXiv:2404.05685 [cond-mat.str-el]
[61] White S R 1992 *Phys. Rev. Lett.* **69** 2863
[62] McCulloch I P and Gulácsi M 2002 *Europhys. Lett.* **57** 852
[63] Calabrese P and Cardy J 2004 *J. Stat. Mech.* **2004** P06002
[64] Wigner E 1934 *Phys. Rev.* **46** 1002
[65] Drummond N D and Needs R J 2009 *Phys. Rev. Lett.* **102** 126402
[66] Azadi S and Drummond N D 2022 *Phys. Rev. B* **105** 245135
[67] Musser S, Senthil T, and Chowdhury D 2022 *Phys. Rev. B* **106** 155145
[68] Musser S and Senthil T 2022 *Phys. Rev. B* **106** 235148